GEOPHYSICS, VOL. 88, NO. 1 (JANUARY-FEBRUARY 2023); P. D1–D12, 13 FIGS., 1 TABLE.
10.1190/GEO2022-0031.1

Improving shallow and deep seismic-while-drilling with a downhole pilot in a desert environment

Ilya Silvestrov[1], Andrey Bakulin[1], Ali Aldawood[1], Emad Hemyari[2], and Anton Egorov[3]

ABSTRACT

Processing seismic data from drillbit-generated vibrations requires a reliable source signature for correlation and deconvolution purposes. Recently, a land field trial has been conducted in a desert environment. A memory-based downhole vibration accelerometer has been used together with a more conventional top-drive sensor to continuously record the pilot signal from 590 to 8600 ft (180–2621 m). Past results indicate that seismic-while-drilling (SWD) data processed using the top-drive accelerometer exhibit good quality in the middle sections of the well but a reduced signal-to-noise ratio for shallow and deep sections. One of the main challenges in using the downhole pilot is a substantial drift of the downhole clock time. To resolve it, a novel automated time-alignment procedure using the GPS-synchronized signal of the top-drive sensor as a reference is applied. The downhole recording provides a source signature of better quality. In shallow sections of the well, it helps to overcome the intense surface-related vibrational noise, whereas, in deeper sections, it provides a cleaner extraction of weaker signals from the polycrystalline diamond compact bits. Processing with the downhole pilot results in better surface seismic data quality than with a conventional top-drive sensor. Therefore, enabling the use of the synchronized downhole pilot signal is of crucial importance for SWD applications. Modern cost-effective near-bit vibrational sensors widely used for different nonseismic applications could be an effective acquisition solution, as shown in this study.

INTRODUCTION

The use of drillbit-generated seismic waves to retrieve subsurface information during the drilling process is a long-standing geophysical problem. Although the appeal is clear, its actual realization faces several technical issues. A breakthrough toward practical applications of this seismic-while-drilling (SWD) technique with a drillbit as a source has been achieved in the 1980s and 1990s by several academia and industry groups (Staron et al., 1988; Miller et al., 1990; Rector and Marion, 1991; Haldorsen et al., 1995; Angeleri et al., 1996; Miranda et al., 1996; Naville et al., 2004; Poletto and Miranda, 2004). The main idea is to transform the continuous chaotic drillbit-generated signals into conventional impulse seismograms through correlation or deconvolution with the source signature similar to the vibroseis technique. For this purpose, most of the developed systems use a pilot signal recorded by a vibrational sensor mounted on a top drive of a drilling rig. The top-drive sensor provides an acceptable estimation of the source signature. However, such a pilot remains significantly affected by the drillstring propagation effects and contaminated by strong noise of surface origin. After a series of field applications of such systems, it has been observed that, in general, SWD data quality varies significantly and depends on several factors, such as geology and drilling conditions. In addition, the increasingly popular polycrystalline diamond compact (PDC) bits excite weaker SWD signals and with less favorable radiation patterns than rollercone bits (see, e.g., Poletto, 2005). All of these issues decrease the usage of the SWD technique with a drillbit signal as a standard service in the industry.

Despite the observed variability in the data quality, the real-time capabilities of such drillbit recordings and some of their unique

Manuscript received by the Editor 20 January 2022; revised manuscript received 19 August 2022; published ahead of production 5 October 2022; published online 5 December 2022.
[1]Saudi Aramco, EXPEC Advanced Research Center, Dhahran, Saudi Arabia. E-mail: ilya.silvestrov@aramco.com (corresponding author); andrey.bakulin@aramco.com; ali.dawood.18@aramco.com.
[2]Formerly Saudi Aramco, EXPEC Advanced Research Center, Dhahran, Saudi Arabia; presently Curtin University, Perth, Australia. E-mail: emad.al-hemyari@postgrad.curtin.edu.au.
[3]Aramco Research Center — Moscow, Aramco Innovations LLC, Moscow, Russia. E-mail: anton.egorov@aramcoinnovations.com.

DOI:10.1190/geo2022-0031.1

properties continue to make the technique very attractive (Bakulin et al., 2020a; Goertz et al., 2020, 2021; Aldawood et al., 2021; Houbiers et al., 2021; Poletto et al., 2022). Compared with conventional vertical seismic profiling (VSP) (Hardage, 2000), one of the benefits of the SWD technique is that no downtime is required once the system is installed prior to drilling. The recordings are done continuously and do not interfere with drilling operations. In addition, there is no need for a seismic source at the rig site, as in the alternative technology of acquiring seismic data while drilling with a source at the surface and receivers in the borehole (Esmersoy et al., 2005). The absence of an active source simplifies operations with the potential of a fully autonomous acquisition. SWD deliverables with a drillbit as a seismic source are similar to conventional VSP outcomes (Poletto and Miranda, 2004; Kumar and Bettinelli, 2021) and include full wavefields, check shot, corridor stack, and images all obtained at or at nearly real-time while drilling. Enabled applications range from a while-drilling look-ahead prediction of formation tops with a decreased uncertainty to accurately positioning the drillbit in seismic time or depth volumes. Such information could facilitate different drilling decisions and aid geosteering. With a trend in the drilling industry toward automation (de Wardt et al., 2012), SWD data can be integrated with other subsurface information for more accurate data-driven decisions during drilling (Saputelli et al., 2003). Apart from applications in the context of drilling, SWD data can be used in exploration or field development. Notably, such an approach allows measurements in shallow sections typically not covered by wireline VSP surveys due to the large borehole's diameter and multiple cemented casings. As a result, critical near-surface information is gathered for more accurate depth mapping of target horizons (Bakulin et al., 2020a; Aldawood et al., 2022). Recent results obtained with large-aperture receiver arrays show a potential usage of drillbit seismic data for look-ahead reservoir imaging to provide relevant information for accurate placement of infill wells (Goertz et al., 2020).

To facilitate the applications, several acquisition and processing techniques have been proposed to improve the estimation of a drillbit-generated signal and arrive at more reliable SWD data. They include signal focusing using large receiver arrays to retrieve deconvolution operators directly from geophone data (Haldorsen et al., 1995) and joint use of different sensor recordings to separate pilot signals using statistical independence (Poletto et al., 2000). However, using downhole pilot sensors is usually considered the most promising approach (Naville et al., 2004; Poletto et al., 2020). In this case, the pilot signal is recorded by accelerometers or other sensors close to the drillbit. Unlike surface pilots from top-drive sensors, the downhole pilot is not significantly affected by drillstring attenuation and propagation effects. Previous studies conducted in some limited depth intervals of 200–400 m around a target show that such recordings can provide a more accurate and stable representation of the pilot signal, increasing the signal level in the data (Miranda et al., 1999; Naville et al., 2004; Poletto and Miranda, 2004; Poletto et al., 2014). However, real-time transmission of downhole pilots requires fast electromagnetic telemetry, which remains costly and not widely available on most drilling rigs. An alternative solution is to use memory-based vibration sensors. Recently, several cost-effective tools to continuously record high-frequency triaxial accelerations directly behind the bit have become readily available. The devices are widely used for drilling dysfunction analysis (Macpherson et al., 2015; Jones and Sugiura, 2020) or rock properties estimation (Haecker et al., 2017; Glubokovskikh et al., 2020), but their application to SWD has not yet been exploited in detail. Their main issue is the significant drift of the downhole clock, which often significantly exceeds the precision required for seismic applications. A possible solution is to use a GPS-synchronized top-drive vibration sensor for time correction (Naville et al., 2004; Egorov et al., 2021). An alternative hardware solution is to use more sophisticated and robust high-precision downhole clocks. For example, Vieitez and Cox (2017) describe tools with a small drift of 1 ms per 10 days used in offshore wells. With further reduction in sensor costs, such a solution could extend to onshore acquisition.

Recently, SWD data have been acquired during testing a prototype DrillCAM system at an onshore well down to 10,000 ft (3048 m) in an arid environment (Bakulin et al., 2020a). The system is comprised of wireless surface geophones accompanied by top-drive and downhole vibration sensors. The downhole pilot is continuously recorded from 590 to 8600 ft (180–2621 m) and only misses the shallowest section above 590 ft. To our knowledge, this is the first usage of a downhole sensor to record pilot for SWD applications for such an extended period, including shallow and deep sections of the borehole, using various drill bits and bottom-hole assembly configurations. Bakulin et al. (2020a) present the acquisition details and some initial applications using the top-drive sensor as a pilot. They show that SWD data obtained using the top-drive accelerometer exhibit good quality in the middle sections of the well and reduced signal-to-noise ratio for shallow and deep sections. Aldawood et al. (2021) present imaging results ahead and around the bit using the top-drive pilot. Silvestrov et al. (2021b) discuss data processing details, including the usage of both pilots, and show some initial results obtained with the downhole pilot. The downhole clock's drift is mitigated by using a data-driven alignment procedure that uses a GPS-synchronized top-drive sensor as a reference (Egorov et al., 2021). The use of the downhole pilot for shallow subsurface characterization is presented by Aldawood et al. (2022), where the low signal-to-noise ratio issue in the geophone-correlated data, typical of arid environments, was resolved by the nonlinear beamforming approach (Bakulin et al., 2020b) used for land seismic data processing.

Following Silvestrov et al. (2021a), this work presents in more detail the results obtained using the downhole pilot signal and their comparison with the top-drive pilot over the whole available depth range. We show that the usage of the downhole pilot leads to significantly higher seismic data quality in the shallow sections compared with the top-drive pilot. However, the usable seismic signal in deeper PDC bit-drilled sections remains undetectable below 6159 ft (1877 m) with the current processing sequence. The structure of the paper is the following: first, we summarize the data acquisition and processing methods used in this study; second, we present a detailed comparison of the top-drive and near-bit pilots' quality in shallow sections drilled with rollercone bits and deeper sections drilled with PDC bits; finally, the processing results of continuous surface seismic geophone data using both types of pilots are presented and discussed.

DATA ACQUISITION AND PROCESSING METHODS

Seismic data were recorded using 2500 vertical component single-sensor geophones installed around the rig, as shown in Figure 1. Each geophone was connected to a wireless transmitter, sending the data in nearly real time to a central recording system inside the rig

DOI:10.1190/geo2022-0031.1

pad. The initial acquisition layout had a square shape with a side length of approximately 1100 m centered around the rig. Two additional orthogonal lines reached a maximum offset of 3000 m (Figure 1). The spacing between the geophones was 25 m in inline and crossline directions. Such a layout was designed for a shallower drilling depth down to 2665 ft (812 m). A different geophones' layout with a smaller central patch size but wider orthogonal lines recorded deeper sections with the same number of sensors. Repositioning of wireless geophones was done during casing/cementing operations. In addition, several lines were deployed in a saw-tooth-like pattern to test additional options for better noise separation during the processing (Bertelli et al., 1998; Poletto and Miranda, 2004). Continuous recording with surface geophones was achieved while drilling from the surface down to 10,000 ft (3048 m). The well diagram for the considered depth intervals is shown in Figure 1c.

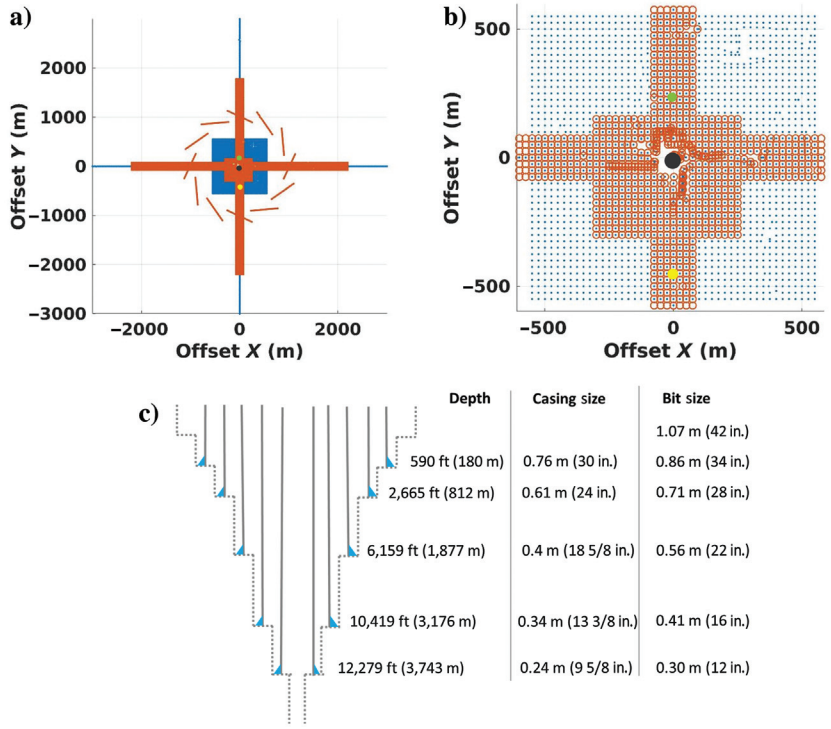

Figure 1. Seismic acquisition geometry used in the field trial: (a) general view and (b) magnified into the central part of the geophone layout around the rig. The rig (the black dot) is located at the origin. Blue dots denote the receiver positions used for SWD when drilling from the surface to 2665 ft (812 m) (drilling runs N 1 and 2 from Table 1). Red dots show the receiver pattern for deeper drilling runs below 2665 ft (812 m). Yellow and green dots show the locations of common-receiver gathers shown in Figures 10 and 12 and discussed in the text. The well diagram showing the casing configuration and the drillbit size is presented in (c).

In addition to the surface geophones, two sets of continuously recording 3C cabled accelerometers were mounted on the top drive to record drillstring vibrations at the surface. At the same time, a memory-based near-bit tool was used to record the drillbit vibrations downhole in most of the drilling runs (Table 1). The downhole tool in this study was equipped with a 3C accelerometer recording radial, axial, and tangential vibrations with a sampling rate of 1500 Hz, measurement range of ± 200 g, and resolution of 0.007 g. The sensors' dynamic characteristics satisfied the main SWD requirements outlined in Table 5.1 by Poletto and Miranda (2004). In addition to the high-frequency vibration data, the tool could record downhole rotary speed or rotations per minute (RPM), temperature, and vibrations at a reduced sampling rate using sensors with higher resolution but reduced dynamic range (not used in this study). More details on the data acquisition aspects of the trial have been provided by Bakulin et al. (2020a). Due to the experimental nature of the prototype system, data processing and interpretation of the results were performed after drilling. The primary analysis goals were to assess the overall feasibility of the SWD system comprised of wireless geo-

Table 1. Overview of the drilling runs and bit types used in the study together with the type of drilled rocks.

Run	Bit size	Bit type	Depth	Downhole sensor	Rock type
1	1.09 m (34 in)	Rollercone	0–590 ft (0–180 m)	No	Mainly composed of anhydrite
2	0.71 m (28 in)	Rollercone	590–2665 ft (180–812 m)	Yes	The top part is a regional aquifer consisting of fractured soft carbonates and the bottom section is highly compacted shale layers
3	0.56 m (22 in)	Rollercone	2665–2677 ft (812–816 m)	Yes	Mainly composed of sandstone
4	0.56 m (22 in)	Rollercone	2677–4180 ft (816–1274 m)	Yes	The top section consists of sandstone and shale interbeds. The lower section consists of highly compacted carbonates.
5	0.56 m (22 in)	PDC	4180–5246 ft (1274–1599 m)	Yes	Mainly composed of sandstone
7	0.56 m (22 in)	Rollercone	5246–6159 ft (1599–1877 m)	Yes	Consists of dense and hard anhydrite
8	0.41 m (16 in)	PDC	6159–7802 ft (1877–2378 m)	Partly yes	Layers of hard dense anhydrite and soft carbonates
9	0.41 m (16 in)	PDC	7802–10419 ft (2378–3176 m)	Partly yes	Thick section of carbonates

DOI:10.1190/geo2022-0031.1

phones, top drive, and downhole vibration sensors, verify the quality of the recorded data, and pave the way for future applications.

In contrast to the synchronized top-drive pilot sensors, raw downhole recordings from the memory-based downhole tool in this study could not be directly used as pilot data for SWD due to the significant internal clock's time delay and drift. A typical interpretation-based clock correction applied by drillers uses time alignment of downhole and surface RPM data and achieves an accuracy of several seconds. However, it is insufficient for SWD applications demanding an accuracy of less than a few milliseconds. To reach the required precision, we use a GPS-synchronized sensor mounted on a top drive as a reference for time alignment, as discussed by Egorov et al. (2021). The first step of the time correction procedure is a search of two scalar parameters — shift s and drift d — to create a linear mapping between the time vector for the near-bit acceleration recording and the synchronized top-drive series:

$$t^{\mathrm{td}} = (1+d)t^{\mathrm{nb}} + s, \tag{1}$$

where quantities t^{td} and t^{nb} are the time series for the top-drive and near-bit sensors, respectively. The search is performed by global minimization of the misfit function,

$$J(d,s) = \sum_{t^{\mathrm{td}}} (E^{\mathrm{td}}(t^{\mathrm{td}}) - E^{\mathrm{nb}}((t^{\mathrm{td}}\text{–s})/(1+\mathrm{d})))^2, \tag{2}$$

representing the difference between vibration energy recorded by top-drive (E^{td}) and near-bit (E^{nb}) sensors and calculated in a sliding window. The linear correction from equation 1 usually aligns the data with the accuracy of a few seconds. To reach the accuracy of less than a few milliseconds required by SWD, we apply a time-variant crosscorrelation analysis similar to the one discussed by Naville et al. (2004), in which the correlations between top-drive and downhole pilots are calculated in some windows. The maximum of the correlations identifies the residual time shifts required to tie the time series from the near-bit and top-drive sensors. Such a two-step procedure achieves the near-bit time accuracy acceptable for SWD applications.

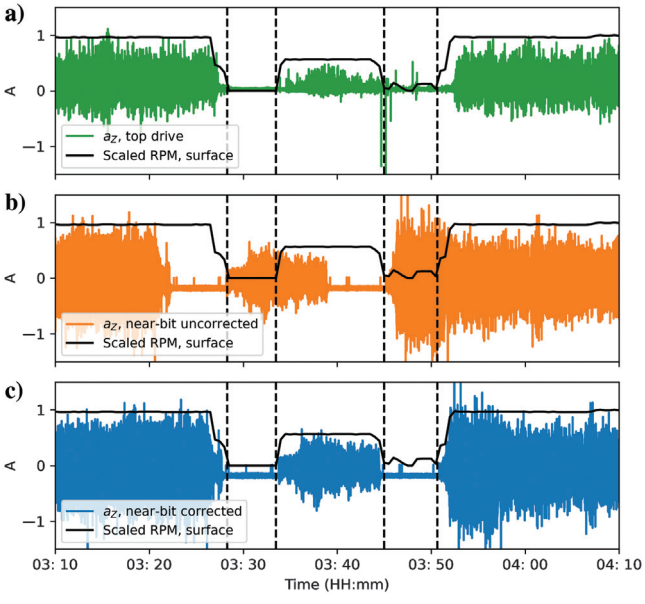

Figure 2. (a) Top-drive vertical accelerometer (a_z) shows accurate alignment with rotation speed RPM data from the electronic drilling recorder at the surface. (b) Near-bit data before time correction is delayed by approximately 6 min. (c) After the time correction, the near-bit data match perfectly the top-drive recordings. Data are taken from drilling run N 5 (Table 1) using the PDC bit. Vertical axes are in relative amplitudes. The acceleration and RPM curves are scaled to make their amplitudes close to one for easy comparison.

Because the top-drive sensor is used as a reference, the aligned downhole pilot also has a delay to the drill-bit signal excitation time corresponding to the signal propagation along the drilling string. Therefore, an additional time correction is introduced into the correlated geophone data at later steps to obtain the actual seismic time, following the usual processing practice with the top-drive pilot (Poletto and Miranda, 2004).

After the alignment step, a standard SWD processing technique (Poletto and Miranda, 2004) using both recorded pilots is applied to these data. That includes correlating the geophone recordings with the pilot signals and stacking the correlated data over some drilling intervals. In the frequency domain, it can be written as

$$U_k(\omega) = \Sigma_{i=1}^{N_k} D_i(\omega)\bar{P}_l(\omega), \tag{3}$$

where D_i is a recorded geophone seismic trace and $\overline{P_i}$ is a recorded pilot signal trace after complex conjugation. The length of each trace before the Fourier transform is 30 s. The number of traces N_k used to produce a single trace at depth level k depends on a drilling rate of penetration (ROP) and a selected drilling depth interval. In the current work, the interval corresponds to a single drillpipe of 30 ft (9.1 m) in length. Assuming a typical penetration rate of approximately 30 ft/h (9.1 m/h), a total of 120 records are stacked together. The stack of the correlated data increases the signal-to-noise level and enables the reconstruction of weak reflection events. Because the seismic wavelength is usually several times larger than the used depth interval, such stacking does not significantly deteriorate the signal waveform.

In addition to the crosscorrelations shown in equation 3, stacked autocorrelations of downhole and near-bit pilots are calculated as

$$\hat{\mathrm{P}}_{\mathrm{k}}(\omega) = \Sigma_{i=1}^{N_k} P_i(\omega)\bar{P}_l(\omega). \tag{4}$$

The autocorrelations are used for quality control and deriving drillstring propagation time corrections. In addition, they are exploited for deriving the pilot deconvolution operators. Together with the direct arrival from the bit, pilot traces recorded either by top-drive or near-bit sensors also contain additional events such as multiples caused by the ends of the drillstring (top drive and drillbit) as well as internal boundaries within (drillstring joints, bottom-hole assembly, etc.). The aim of deconvolution, applied to the correlated data, is to shorten the source signature and attenuate these multiple reflections and other delayed and periodic components recorded by the pilot sensors. Following Poletto and Miranda (2004), we construct a deconvolution operator $\Phi_{\mathrm{k}}(\omega)$ from the stacked autocorrelations of the pilot traces (see equation 4) using Wiener least-squares predictive filtering with unit prediction distance. In time, the operator is reversed to remove anticausal components in the pilot autocorrelation and associated events in the correlated data. The operator length is calculated to include short- and long-period multiples originating in the bottom-hole assembly and the drill pipe and is equal to 2 s in

DOI:10.1190/geo2022-0031.1

the current examples. Finally, the deconvolved SWD data can be written as

$$\hat{U}_k(\omega) = \Phi_k(\omega)\Sigma_{i=1}^{N_k} D_i(\omega)\bar{P}_l(\omega). \quad (5)$$

At the later stages of the data processing flow, we apply additional noise attenuation and data-enhancement procedures based on nonlinear beamforming (Bakulin et al., 2020b). Such enhancement is typical for processing the single-sensor seismic land data in a desert environment. It increases the strength of the weak signal and suppresses the groundroll and other noise. Silvestrov et al. (2021b) provide more information about the processing sequence.

RESULTS

Downhole time correction

Although surface geophones and cabled top-drive sensors have been GPS synchronized in this field study, the downhole vibrations have been recorded using memory-based tools with an internal clock without an accurate start time and subject to significant drift reaching 30–40 min over some of the longer drilling runs. Figure 2a compares the vertical acceleration component recorded by the top-drive sensor with the scaled surface RPM. Note a good match between nondrilling intervals characterized by a low level of vibrations and near-zero RPM values. In contrast, the orange curve in Figure 2b displays the near-bit vibration data clearly delayed by approximately 6 min. After applying the automated data-driven time alignment algorithm that minimizes the misfit in equation 2 and performs additional time-variant crosscorrelation corrections, the revised blue curve in Figure 2c matches the top-drive recordings. In principle, the alignment could be completed purely by the crosscorrelation analysis. However, such a solution would be inefficient due to the significant and unknown initial time shifts (tens of minutes) and long-lasting drilling runs reaching tens of hours. The adopted two-stage procedure provides an initial raw alignment based on the energy attribute followed by a cross-correlation of traces with a reasonable window length and a time lag, making the procedure more practical. We refer the readers to Egorov et al. (2021) for an in-depth description of this alignment procedure and examples.

Pilot signals comparison

As a first step, we compare the quality of raw-recorded top-drive and downhole pilots. Figure 3 shows both signals (after time alignment) recorded in the middle of a shallow drilling run N 2 (Table 1) within the depth interval from 1157 ft (352 m) to 1575 ft (480 m). The continuous data are spliced into 30 s long seismic traces. Root-mean-squared (rms) amplitudes of each trace quantify energy levels recorded by both pilots. Low rms values correspond to pauses in drilling, as confirmed by the drilling indicator from the surface electronic drilling recorder. The indicator matches, in this case, with a bit-on-bottom indicator showing the intervals in which the bit depth equals the borehole depth. The drilling stops during drillpipes connections, as can be identified by stair-like jumps in the drillstring length curve and during periods with low RPM (Figure 3c). We observe a generally good alternation match between both pilots' drilling and nondrilling intervals. Simultaneously, the downhole recordings show a smoother energy distribution within drilling intervals, as manifested by less variable rms curves and more uniform amplitudes and frequency spectra within the traces.

Figure 4 shows the mean and standard deviations of the rms amplitudes calculated for all drilling runs using a sliding window of 75 min. Substantial variability of vibration amplitudes recorded by the top-drive sensor is observed in the shallow drilling run N 2 from 590 ft (180 m) to 2665 ft (812 m), with the standard deviation exceeding 20 dB. As for the downhole sensor, standard deviations are significantly less and are mainly smaller than 5 dB. That might be attributed to the strong rig vibrations at the surface when drilling shallow sections, which manifested as additional noise in the top-drive pilot. In contrast, the downhole tool, recording vibrations near the bit, provides less variable data suggesting that the fluctuations in the top-drive data are not associated with the drillbit noise.

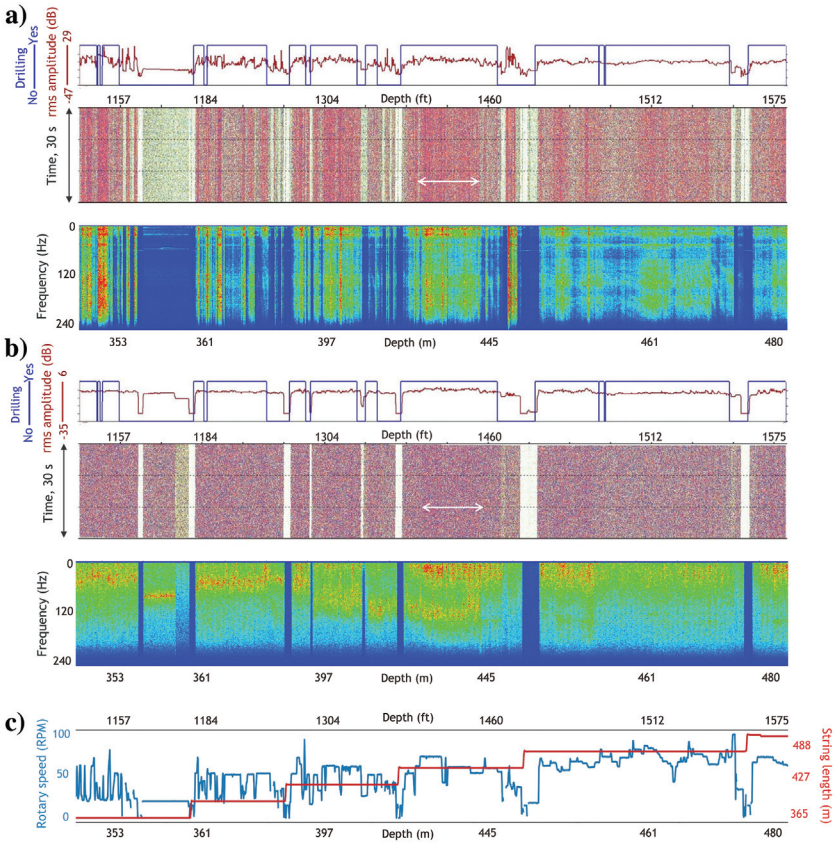

Figure 3. A subset of (a) top-drive and (b) downhole 30 s long pilot traces together with their spectra recorded during shallow drilling run N 2 from 1157 ft (352 m) to 1570 ft (480 m). The corresponding rotary speed and the drillstring length are shown in (c). Note the higher amplitude and frequency variability of the top-drive signal in contrast with the more uniform recordings of the downhole sensor. White arrows in (a and b) show the traces inside the drilling interval with a constant drillstring length as shown in (c) used for spectrum analysis in Figure 5.

The pilots' amplitude spectra confirm this observation (Figures 3 and 5). The spectrum of the top-drive signal has substantial variability, with several frequency peaks over the entire seismic frequency range. For example, a strong peak frequency identified in the top-drive pilot at approximately 45 Hz and not observable in the downhole or surface geophone data averaged over the same drilling interval (Figure 5) can be interpreted as a manifestation of the additional noise component in the top-drive pilot. Conversely, the downhole pilot spectra show a much smoother and consistent behavior, less affected by significant variations and peak frequencies. A low-frequency amplitude drop in the downhole data is caused by the low-cut filtering with a 4 Hz cut-off frequency used during the time-alignment step.

Looking into the deeper sections, the mean energy level of both pilots is comparable until the end of run N 5 at a depth of 5246 ft (1599 m) (Figure 4). Below 5264 ft, the energy level recorded by the top-drive sensor is consistently and significantly less than that of the vibrations recorded by the downhole tool. Both pilots exhibit a substantial decrease in the amplitudes recorded after run N 7 at a depth of 6159 ft (1877 m). Such a reduction may be attributed to the "less

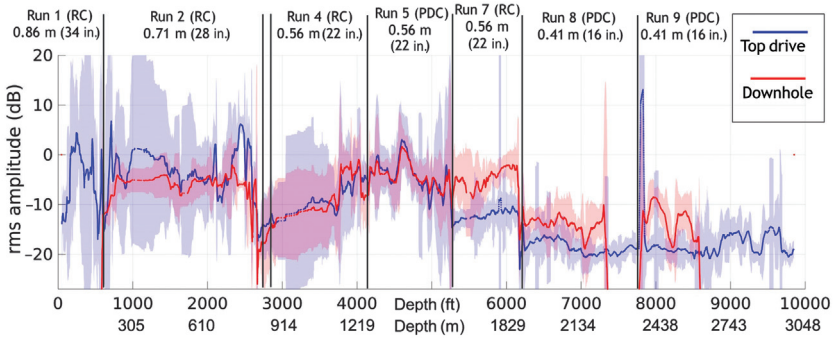

Figure 4. Mean (the solid lines) and standard deviations (the shaded area) of the rms amplitudes for top-drive and downhole pilots calculated in a sliding window of 75 min during drilling intervals only. Note more considerable amplitude variations (high standard deviations) of the top-drive data in the shallow part (runs N 2 and 4). In addition, note the lower mean amplitude level of top-drive sensor data in the deeper part (from run N 7 and below).

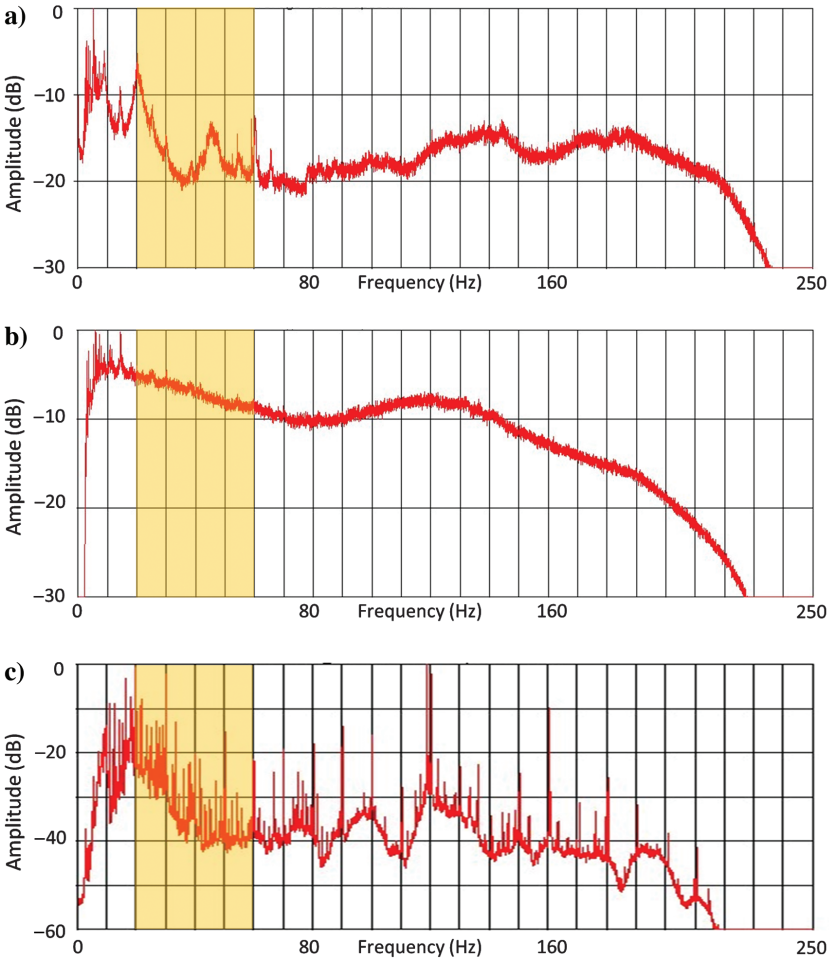

Figure 5. Average power spectra of the (a) top-drive and (b) downhole pilot signals from the shallow drilling interval marked with the white arrows in Figure 3. Note more uniform energy distribution versus frequency for downhole data with fewer peak frequencies. A low-frequency amplitude drop in the downhole data is caused by the low-cut filtering with a cut-off frequency of 4 Hz used during the time-alignment step. A trace spectrum recorded by a surface geophone at a distance of 475 m from the well is shown in (c) for comparison. Yellow areas indicate the effective bandwidth of data after processing.

DOI:10.1190/geo2022-0031.1

loud" nature of the PDC bit with smaller diameters (less than 16 in) used from this depth. PDC bits have been reported to generate less seismic signal than rollercone bits, thus making them less favorable for SWD (Poletto and Miranda, 2004).

Nevertheless, successful examples of SWD with PDC bits exist offshore (Goertz et al., 2021), even though the exact reasons why it works in one case and not in the other are still to be understood. Notably, the 22 in (0.56 m) PDC bit used in run N 5 provides a strong vibration energy level recorded by the top-drive and downhole sensors. In general, the level of the recorded drillbit vibrations depends on many factors, such as the drilling regime, rock hardness, and bottom-hole assembly configuration. A detailed analysis of the recorded drillstring vibrations is a topic of a separate study. However, Figure 4 strongly suggests that the downhole sensor can record a more stable pilot signal with a greater energy level and higher quality than the top-drive accelerometer.

A typical practice to evaluate the pilot signal's quality is to analyze its autocorrelations (Poletto and Miranda, 2004). Figure 6a and 6b shows pilot autocorrelations after stacking along 30 ft depth intervals corresponding to the length of a one drillpipe and pilot deconvolution following a standard processing practice (Poletto et al., 2014). Additional median filtering is applied to remove short-period reverberations. The strong dipping events are the long-period multiples propagating along the drillstring and bouncing between its top and bottom (Poletto et al., 2001). These multiples allow assessing the overall signal-to-noise ratio of the recorded pilot signals. In Figure 6c and 6d, we additionally stack the traces over 90 ft intervals corresponding to a constant drillstring length to make it more transparent. The multiples are aligned horizontally using time shifts based on the drillbit depth and the drillstring velocity of 4880 m/s, calculated using the long-period multiples' slope shown in Figure 6a and 6b. The signal level is reasonable in both pilots in the middle sections between approximately 2000 ft (609 m) and 6200 ft (1890 m). In the shallow part, the top-drive signals are overwhelmed by intense noise, similar to Figure 2, observable as substantial waveform variations in Figure 6c. The multiple events visible in the downhole pilot are much more coherent. They can be tracked up to the shallowest depth of 590 ft (180 m) recorded with the downhole sensor (Table 1). The top-drive pilot does not reveal any signal in the deeper part below 6200 ft (1890 m). These sections have been drilled with 16 in (0.41 m) PDC bits, highlighting the known chal-

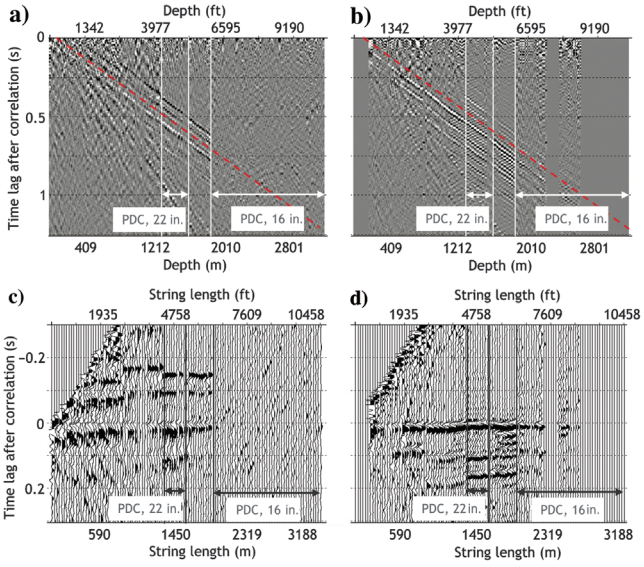

Figure 6. Autocorrelations of (a) top-drive and (b) downhole pilot signals after stacking along 30 ft depth interval corresponding to a one drillpipe, pilot deconvolution, median filtering, and band-pass filtering. Each trace is normalized individually with respect to its maximum value. Note long-period drillstring multiples (underneath the red lines) indicating the quality of the pilot signal. (c) For the top-drive and (d) for the downhole pilots, these multiples are aligned horizontally at zero time lag using static shifts with a drillstring velocity of 4880 m/s, and the traces are additionally stacked over three drillpipes corresponding to a constant drillstring. In the top-drive pilot, the multiples are noisy in the shallow part and completely absent in the deeper section drilled with a PDC bit. In the downhole autocorrelations, the multiples are strong and coherent, mostly from the top to the bottom of the recorded depth interval.

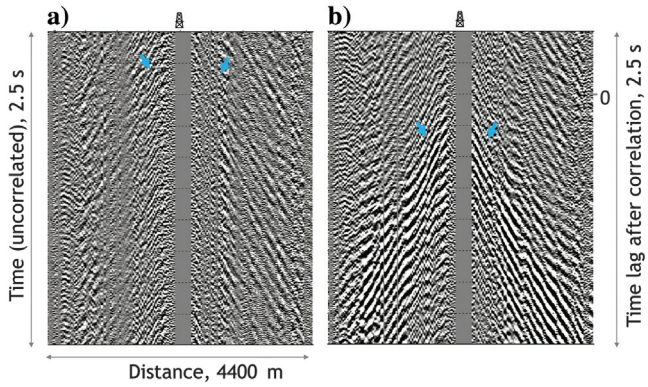

Figure 7. Common-bit gathers along the central west–east line recorded while drilling at a depth of 3860 ft (1176 m): (a) uncorrelated raw data and (b) data after correlation with the downhole pilot. Raw data in (a) exhibit continuous seismic events interpreted as surface waves (marked with the blue arrows) coming from the rig located in the line center. Correlation with the downhole pilot signal helps compress these events in (b), as shown by the blue arrows, and produces conventional impulsive seismograms with the source at the bit's position. Gather is obtained during drilling run N 4 with the rollercone bit (Table 1).

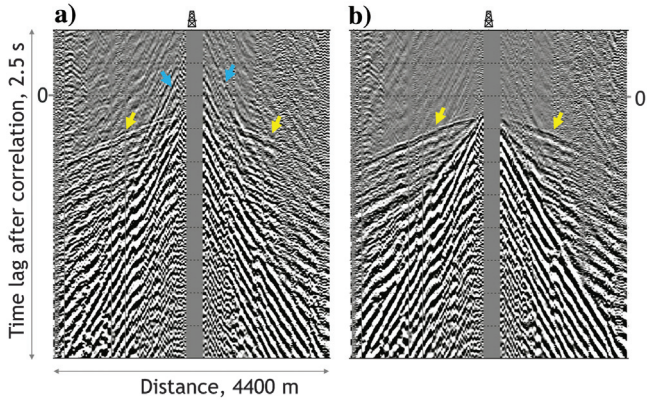

Figure 8. (a) Stacking correlated data over a single 30 ft (9.1 m) drillpipe (approximately 1 h of recordings) increases the signal-to-noise ratio and reveals a direct arrival event, marked with the yellow arrows. Blue arrows show correlation-related noise preceding direct arrivals. (b) Same data but after pilot deconvolution exhibiting attenuation of such noise and providing more clear and focused direct arrivals.

lenge of the SWD technique with such kinds of bits. In contrast, the downhole pilot autocorrelations contain coherent multiple events for deeper runs with PDC bits between 6200 ft (1890 m) and 7300 ft (2225 m). The weaker but coherent signal remains visible at more considerable depths between approximately 7800 ft (2377 m) and approximately 8500 ft (2590 m). The autocorrelation diagnostic confirms that the downhole vibration sensor provides the pilot signal of better quality and a higher signal-to-noise ratio.

Surface SWD data

A significant amount of energy observed in the SWD records is the noise from the rig's structure, mud shakers, engines, vehicles, generators, etc. Figure 7a shows raw data from a central east–west line recorded at the surface during drilling run N 4 at 3860 ft (1176 m). The rig structure in the middle of the line induces intense linear seismic events propagating away from the pad. The correlation of the raw data with the downhole pilot reveals strong surface waves usually observed in conventional land seismic data (Figure 7b). The main target signals of the SWD technique are direct arrivals and reflected waves induced by the drillbit in the subsurface and recorded at the surface. A vertical stack of the correlated data over a specific drilling depth interval is performed to increase these weak signals. We apply a stack over one drillpipe length equal to 30 ft, i.e., a single 9.1 m pipe length. They combine approximately 1 h of uncorrelated recordings into a single gather, assuming a typical penetration rate of approximately 30 ft/h (9.1 m/h). The data after vertical stacking reveal a weak direct-arrival event, shown in Figure 8a. In addition to the first arrivals from the bit, pilot traces recorded either by top-drive or near-bit sensors contain additional events such as multiples caused by the ends of the drillstring (top drive and drillbit) as well as internal boundaries (drillstring joints, sections of the bottom-hole assembly, etc.). Pilot deconvolution applied to the correlated and stacked data removes the pilot-filtering effects reversed in "backward time" and strongly attenuates seismic events introduced by pilot signals before first arrivals, as shown in Figure 8b. Note that the near-offset arrivals are clearly visible in this gather, usually masked by rig-radiated noise. Because the downhole pilot is aligned with the top-drive pilot located at the top of the drillstring, an additional time correction is applied to the correlated geophone data to account for the propagation time of the drillbit signal along the drillstring from its bottom to top. As discussed previously, this correction is based on the drillbit depth and the effective drillstring velocity. Finally, filtering with a passband from 20 to 60 Hz is applied to remove the low-frequency groundroll-type noise from the seismic records. Alternatively, more sophisticated noise attenuation algorithms might be used similar to conventional land-data processing flows, at least for low frequencies, where the groundroll noise is not aliased. Conventional geophone arrays also can be used as an alternative to improve the signal-to-noise ratio.

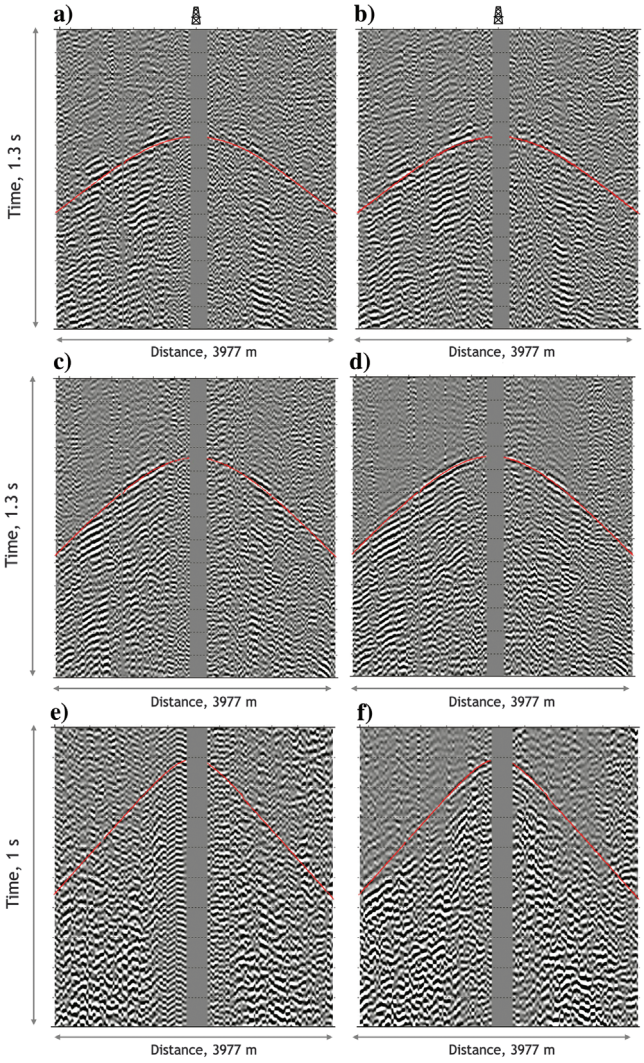

Figure 9. The SWD common-bit/shot gathers recorded along a central west–east line after complete processing a top drive (a, c, and e) and a downhole pilot (b, d, and f) shown at various depths: (a and b) 4410 ft (1344 m) from drilling run N 5 with PDC bit, (c and d) 3182 ft (970 m) from drilling run N 4 with a rollercone bit, and (e and f) 930 ft (283 m) from drilling run N 2 with a rollercone bit (Table 1). The red lines show synthetic first-arrival traveltimes calculated using a legacy velocity model from nearby wells.

Figure 9 shows processed common-shot gathers recorded at different drilling depths along the west–east central line. A crossline stacking in the south–north direction of seven adjacent receiver lines is additionally applied to enhance the single-sensor recordings' signal level. Both pilots provide comparable seismic data at a depth of 4410 ft (1344 m) from drilling run N 5 with a 22 in PDC bit (Figure 9a and 9b). Direct arrivals are clearly visible. They match reasonably well with synthetic traveltimes calculated using a legacy 1D velocity model from a nearby well. At a shallower depth of 3182 ft (969 m) (Figure 9c and 9d, drilling run N 4 with the 22 in rollercone bit), both pilots also lead to SWD records of good quality. However, the top-drive result is noisier, as can be seen at near offsets, where the direct arrivals cannot be tracked in Figure 9c in contrast to the ones in Figure 9d obtained with the downhole pilot. The data at a shallow depth of 930 ft (drilling run N2 with 28 in rollercone bit), produced using the top-drive and downhole signals, exhibit even more pronounced differences (Figure 9e and 9f). The top-drive pilot fails to provide a reasonable seismic gather in this case. In contrast, the downhole pilot still leads to good-quality data with coherent first arrivals at near offsets. For larger offsets, refracted arrivals also become clearly visible. These observations are consistent with the observed quality of the pilots themselves (Figures 3–6). The top-drive recordings are noisier in the shallow part and hence fail to accurately estimate the drillbit

DOI:10.1190/geo2022-0031.1

source signature, leading to the deterioration of final SWD seismic data. At deeper depth levels, where the top-drive sensor still provides a pilot of reasonable quality, we observe a much better quality of near-offset traces processed with the downhole pilot. This is of direct practical importance for checkshot and other applications. Note the lack of signal at near offsets in Figure 9a and 9b, where a PDC drillbit was used, which can be attributed either to a more substantial rig-generated noise or to a specific PDC bit's radiation pattern different from the vertical force pattern typical of roller-cone bits.

The quality of processed SWD data varies with depth, as shown by the checkshot gathers in Figure 10. Due to the similarity of the SWD experiment to a reverse VSP survey, the checkshot corresponds to a common-receiver gather. It has been recorded at an offset of 450 m to the south from the rig with relatively good data quality. The top-drive pilot leads to a robust checkshot gather in the depth interval between approximately 3000 ft (914 m) and approximately 6100 ft (1859 m) (Figure 10a). Above 3000 ft (914 m) depth, the traces become much noisier with hardly trackable direct arrivals. In contrast, the data processed with the same flow but using a downhole pilot provide SWD records with a reliable and clearly visible direct wave from approximately 1400 ft (426 m) depth (Figure 10b). First-arrival traveltimes picked from these gathers and the corresponding inverted velocity profiles are shown in Figure 11. The checkshot gather obtained with the top-drive sensor does not allow picking the direct wave above 2000 ft (609 m) (the red line). In addition, the picks between 2000 ft (609 m) and 3000 ft (914 m) are characterized by a low confidence level. In contrast, high-confidence picks can be derived from 1400 ft (426 m) using SWD data obtained with the downhole pilot. Although less confident, visible direct arrivals still support picking first breaks as shallow as approximately 1000 ft (304 m). Application of a nonlinear beamforming (NLBF) data enhancement algorithm (Bakulin et al., 2020b) with an array size of 9 × 9 receivers or 240 m × 240 m (Figure 10c) leads to additional improvement of the signal-to-noise ratio for all depth levels and further helps to reveal the shallower section above 1000 ft (304 m). A good match between the picks from the SWD data and conventional VSP picks from a nearby well confirms the robustness of the while-drilling checkshot. In general, the inverted velocity profiles agree with each other. However, the top-drive pilot provides a considerably more oscillating velocity with some variations not observable in other models that can be attributed to a more significant pick uncertainty. Note that several shallowest picks in legacy VSP traveltime curves have been deemed unreliable. They exhibit a staircase behavior above 2000 ft (610 m) potentially caused by multiple shallow casing strings (as shown in Figure 1c) with imperfect cementation. Bad picks lead to unfeasible velocity oscillations. In contrast, the downhole data show very reasonable and smooth behavior in this part.

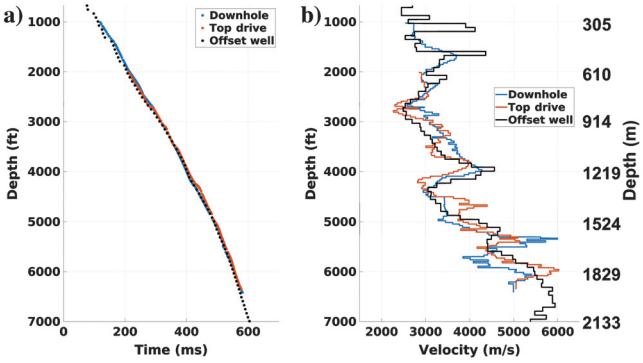

Figure 11. (a) Verticalized time-depth curves picked from the data shown in Figure 10a and 10b at 450 m offset and (b) the corresponding inverted velocity profiles. The data processed using a top-drive sensor do not support reliable picking above 2000 ft (610 m) (the red line). In contrast, the data processed using the downhole sensor provide picks up to 1000 ft (305 m) depth (the blue line). Traveltime curves and inverted velocities agree with the conventional VSP in a nearby well (the black line).

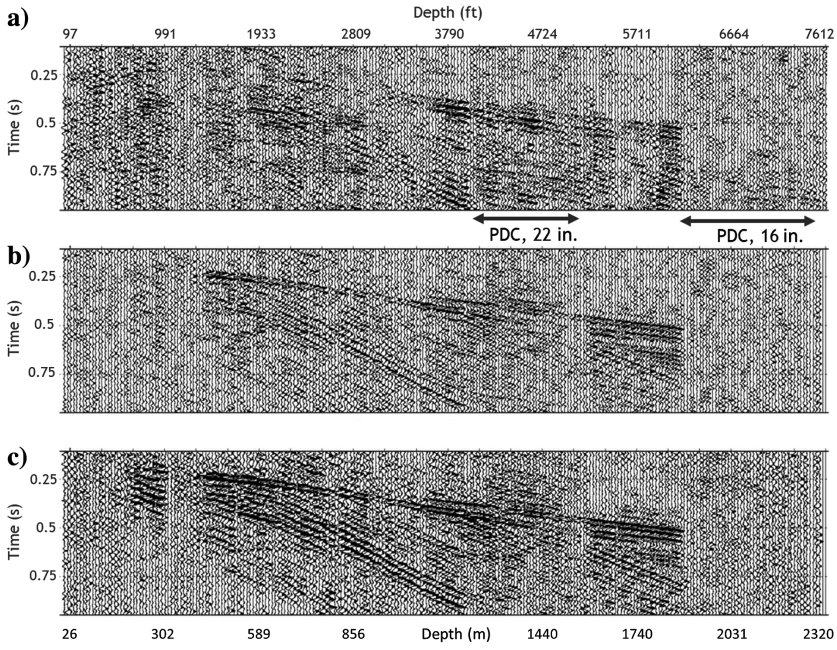

Figure 10. The SWD common-receiver gathers or checkshots obtained with different pilot signals using a receiver patch with the offset of 450 m to the south from the rig (marked with the yellow dot in Figure 1): (a) top-drive pilot and (b and c) downhole pilot. To increase the signal-to-noise ratio, traces from seven receivers (1 × 7 crossline patch) are stacked in (a) and (b). In addition, nonlinear beamforming with an aperture of 9 × 9 receiver stations is applied to enhance the data in (c).

DOI:10.1190/geo2022-0031.1

Better quality of the first-arrival events in the shallow section can be observed at a closer offset of 200 m, as shown in Figure 12. As in the previous geophone location, the quality of the data processed with the top-drive pilot is low in the shallow section, even after the NLBF application (Figure 12a). The downhole pilot allows revealing clear direct waves for most depth levels, including those in the very shallow section (Figure 12b and 12c). The shallowest depth with a reasonable data quality observed in the case is 686 ft (209 m), only 100 ft (30 m) below the starting depth of the first downhole recordings (Table 1). This extremely shallow depth is usually out of reach for standard VSP acquisitions. Therefore, dedicated uphole surveys are usually conducted to measure the time-depth relations for near-surface characterization at such depths. We plan to record downhole data from the surface to check if such an SWD checkshot can completely replicate the uphole survey in future trials.

DISCUSSION

The presented case study shows that processing surface data acquired while drilling using a pilot from a downhole near-bit sensor provides much better data quality than using a pilot from a conventional top-drive sensor. The memory-based downhole near-bit sensors are cost effective and readily available in the drilling industry. The most significant improvement in the presented case study is achieved in a shallow depth above 3000 ft (914 m). We attribute it to a better quality of the near-bit pilot recordings due to the lower susceptibility to surface-generated noise. Conversely, the top-drive pilot sensor is strongly contaminated by various noise sources at the surface, including the rig's structure vibrations, thus providing an overall noisier pilot. A lower-amplitude signal in the near-surface section between approximately 1000 ft (304 m) and 1400 ft (426 m) consistently observed in all the SWD gathers (Figures 10 and 12) is attributed to a known soft carbonate formation drilled with a high penetration rate, as shown in Figure 12d, generating a lower level of seismic signal when crushed by the drillbit.

Autocorrelation analysis of pilot data at deep intervals drilled with PDC bits of the smaller diameter of 16 in reveals that the near-bit sensor continues to provide a reasonable pilot, whereas the top-drive pilot fades away. However, SWD data obtained with both pilots do not show identifiable direct arrivals at this depth. We interpret this as the drillbit signal below 6159 ft (1877 m) becoming too weak compared with the surrounding noise. To illustrate this, we use the full focusing capability of the 2500 geophones array to detect very tiny signals analogous to the analysis of Kostov (1990). Assuming a horizontally layered medium in the borehole's vicinity, we calculate semblance coherency measures along 3D hyperbolic moveout as in conventional velocity analysis (Figure 13). In contrast to the work by Kostov (1990), where uncorrelated data were used as an input, and the time-invariant trajectories were parameterized by pseudodepth and velocity, here we use correlated and fully processed data to compute velocity spectra. A good focus of the direct-arrival event is observed at the end of the drilling run N 7 drilled with the 22 in rollercone bit. Focusing traveltime coincides nicely with the checkshot. However, in an interval drilled with a 16 in PDC bit, only 80 m below, no reliable direct arrival can be found even using the entire 2500 fold array. Despite these observations, some PDC bits could generate a strong and good-quality

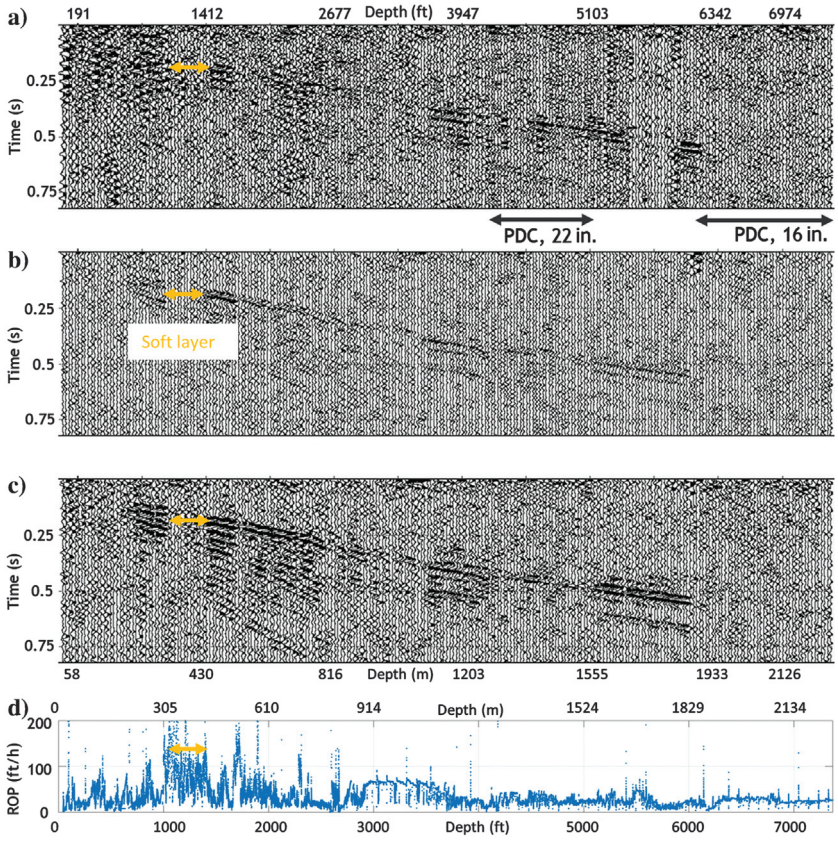

Figure 12. The SWD common-receiver gathers or checkshots obtained with different pilot signals using a different receiver patch with the offset of 200 m to the north from the rig (marked with the green dot in Figure 1): (a) top-drive pilot, (b) and (c) downhole pilot. To increase the signal-to-noise ratio, traces from seven receivers (1 × 7 crossline patch) are stacked to obtain the data in (b). In addition, nonlinear beamforming with an aperture of 9 × 9 receivers' stations is applied to enhance the data in (a) and (c). A high ROP between 1000 ft (304 m) and 1400 ft (427 m) depth, as shown by the orange arrows in (d), is attributed to a soft carbonate formation. A less competent formation leads to lower seismic signals induced by the drillbit and produces lower quality SWD data.

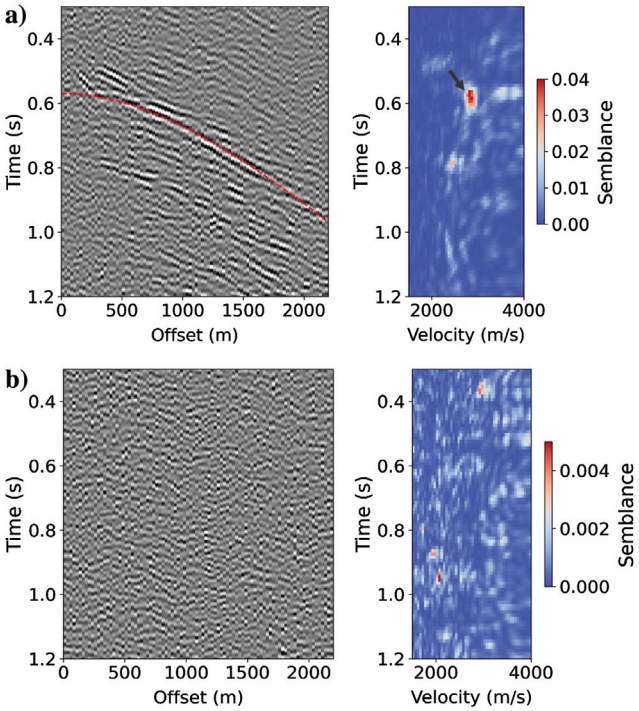

Figure 13. Detection of drillbit signals from the rollercone and PDC bits using coherency analysis: (a) processed data from a 22 in rollercone bit at a depth of 6123 ft (1866 m) and semblance coherency panel calculated along hyperbolic moveout curves; the marked direct arrival event is clearly identified on both displays; (b) data acquired at 6379 ft (1944 m) depth drilled with a 16 in PDC bit. Observe no clear evidence of coherent events that can be interpreted as a direct arrival here, suggesting that the drillbit signal is below the noise level. For visualization purposes, all surface geophones are sorted with respect to offset and stacked into 25 m regular offset bins on the left.

seismic signal, such as the larger 22 in PDC bit used during run N 5. This suggests that the current processing approach might have reached its limits. Regaining the signal in these more challenging conditions requires further investigation. Precorrelation processing of the data is one of the strategies to be considered.

CONCLUSION

We present a field trial of an SWD system in a desert environment and focus on the usage of the downhole pilot, recorded with a memory-based downhole vibration sensor. Such a pilot is continuously recorded in the interval of 590–8600 ft (180–2621 m) and applied for processing the surface geophone data. One of the main challenges in using such a pilot is the substantial drift of the downhole clock. The accuracy required for seismic data processing is less than a few milliseconds. It is significantly more stringent than the requirements of more conventional applications of near-bit sensors, such as drilling dynamics analysis for drilling optimization. The automated data-driven alignment procedure has been successfully applied to these data using a GPS-synchronized top-drive vibration sensor as a reference. After the alignment, the downhole sensor delivers more stable and less noisy pilot data than the top-drive counterpart, especially in shallow drilling sections. At deeper depths, where PDC bits were used, the autocorrelation of the downhole near-bit sensor data exhibits robust long-period drillstring multiples that are completely invisible in the top-drive sensor. Such observation also suggests better quality of the downhole pilot in deeper sections. The downhole pilot is successfully applied for correlation and deconvolution of surface geophone data. Improved SWD gathers validate better quality of the drillbit signature recording with the downhole sensor. In particular, it is demonstrated that such a pilot provides significantly higher SWD data quality in the shallow part (up to 686 ft or 209 m), where the top-drive pilot remains strongly contaminated by surface-related noise.

This work shows that modern cost-effective near-bit vibrational sensors can accurately record a drillbit source signature required to process SWD data for long drilling intervals. Usage of the downhole pilot in the shallow section enables accurate characterization of near-surface velocities potentially to the surface. SWD data can complement conventional VSP surveys that suffer from multiple casing strings in shallow sections and struggle to deliver reliable near-surface velocity profiles. In essence, such SWD checkshot with the downhole sensor can become a proxy for a deep seismic uphole. With continuing advances in fast downhole telemetry, the downhole pilot also may become accessible for real-time applications.

Future work may examine the combined use of the top-drive and downhole pilots. In addition, it could be interesting to analyze data from the remaining surface geophones installed within a rig pad and offset walkaround line with a saw-tooth pattern. Furthermore, a more in-depth analysis is required to relate the strength and radiation pattern of the drillbit source as a function of bit type, size, etc., with the signal-to-noise ratio observed in the SWD records, especially the ones drilled with PDC bits. Finally, more advanced processing sequences and additional applications might be considered, including those based on uncorrelated data.

ACKNOWLEDGMENTS

We would like to thank F. Poletto for sharing his experience and advice during the study. We also are grateful to C. Kostov, A. Goertz, and an anonymous reviewer for their comments and suggestions during the peer review process that helped to improve the paper.

DATA AND MATERIALS AVAILABILITY

Data associated with this research are confidential and cannot be released.

REFERENCES

Aldawood, A., M. Almarzoug, I. Silvestrov, and A. Bakulin, 2022, Characterizing shallow subsurface using 3D seismic while drilling with a downhole pilot: The Leading Edge, **41**, 304–312, doi: 10.1190/tle41050304.1.

Aldawood, A., E. Hemyari, I. Silvestrov, and A. Bakulin, 2021, Imaging ahead of and around the bit in a desert environment: DrillCAM field trial with wireless geophones and top-drive sensor: The Leading Edge, **40**, 374–381, doi: 10.1190/tle40050374.1.

Angeleri, G. P., S. Persoglia, F. Poletto, and F. Rocca, 1996, Process and device for detecting seismic signals in order to obtain vertical seismic profiles during bore drilling operations: U.S. Patent 5,511,038.

Bakulin, A., A. Aldawood, I. Silvestrov, E. Hemyari, and F. Poletto, 2020a, Seismic-while-drilling applications from the first DrillCAM trial with wireless geophones and instrumented top drive: The Leading Edge, **39**, 422–429, doi: 10.1190/tle39060422.1.

Bakulin, A., I. Silvestrov, M. Dmitriev, D. Neklyudov, M. Protasov, K. Gadylshin, and V. Dolgov, 2020b, Nonlinear beamforming for enhancement of 3D prestack land seismic data: Geophysics, **85**, no. 3, V283–V296, doi: 10.1190/geo2019-0341.1.

Bertelli, L., F. Miranda, F. Poletto, and F. Rocca, 1998, Design of SWD 3D RVSP using seisbit technology: 60th Annual International Conference and Exhibition, EAGE, Extended Abstracts, cp-110-00197, doi: 10.3997/2214-4609.201408296.
de Wardt, J., C. D. Chapman, and M. Behounek, 2012, Well construction automation — Preparing for the big jump: Presented at the Applied Technology Workshop on Well Construction Automation, SPE, Extended Abstracts, SPE-163146-MS.
Egorov, A., I. Silvestrov, A. Bakulin, and P. Golikov, 2021, Research note: Automated data-driven alignment of near-bit and top-drive vibration sensors for seismic while drilling and beyond: Geophysical Prospecting, **69**, 1560–1568, doi: 10.1111/1365-2478.13119.
Esmersoy, C., A. Hawthorn, C. Durrand, and P. Armstrong, 2005, Seismic MWD: Drilling in time, on time, it's about time: The Leading Edge, **24**, 56–62, doi: 10.1190/1.1859702.
Glubokovskikh, S., A. Bakulin, R. Smith, and I. Silvestrov, 2020, Machine learning algorithms for real-time prediction of the sonic logs based on drilling parameters and downhole accelerometers: 90th Annual International Meeting, SEG, Expanded Abstracts, 405–409, doi: 10.1190/segam2020-3427085.1.
Goertz, A., B. Atkinson, T. Thiem, and E. V. Bergfjord, 2020, Reservoir imaging-while-drilling with PRM arrays: First Break, **38**, 77–83, doi: 10.3997/1365-2397.fb2020083.
Goertz, A., B. Atkinson, T. Thiem, E. V. Bergfjord, M. Oldervoll, J. Haugestauland, G. Kocsis, and H.-A. Knoop, 2021, Real-time lookahead imaging with drill-bit seismic in the central North Sea: First Break, **39**, 61–68, doi: 10.3997/1365-2397.fb2021084.
Haecker, A., J. Lakings, E. Marshall, J. Ulla, and A Novel, 2017, Technique for measuring (not calculating) Young's modulus, Poisson's ratio and fractures downhole: A Bakken case study: Presented at the 58th Annual Logging Symposium, SPWLA.
Haldorsen, J. B. U., D. E. Miller, and J. J. Walsh, 1995, Walk-away VSP using drill noise as a source: Geophysics, **60**, 978–997, doi: 10.1190/1.1443863.
Hardage, B. A., 2000, Vertical seismic profiling: Principles: Elsevier.
Houbiers, M., S. Bussat, F. Schopper, and F. Hansteen, 2021, High-precision drill bit tracking: International Drilling Conference and Exhibition, SPE/IADC, SPE-204039-MS.
Jones, S., and J. Sugiura, 2020, Analysis of surface and downhole drilling dynamics high-frequency measurements enhances the prediction of downhole drilling dysfunctions and improves drilling efficiency: Abu Dhabi International Petroleum Exhibition and Conference, SPE, Extended Abstracts, SPE-202859-MS.
Kostov, C., 1990, Multichannel seismic experiment with a drillbit source: Ph.D. thesis, Stanford University.
Kumar, R., and P. Bettinelli, 2021, Borehole seismic: Essential contributions over the oilfield lifecycle: Middle East Oil & Gas Show and Conference, SPE, Extended Abstracts, SPE-204889-MS.
Macpherson, J. D., P. Paul, M. Behounek, and R. Harmer, 2015, A framework for transparency in drilling mechanics and dynamics measurements: Annual Technical Conference and Exhibition, SPE, Extended Abstracts, SPE-174874-MS.
Miller, D., J. Haldorsen, and C. Kostov, 1990, Methods for deconvolution of unknown source signatures from unknown waveform data: U.S. Patent 4,922,362.
Miranda, F., L. Aleotti, F. Abramo, F. Poletto, A. Craglietto, S. Persoglia, and F. Rocca, 1996, Impact of seismic while drilling technique on exploration wells: First Break, **14**, 55–68, doi: 10.3997/1365-2397.1996004.
Miranda, F., F. Poletto, F. Abramo, A. Craglietto, and G. Bernasconi, 1999, SWD surface and downhole pilot recording to improve PDC bit signals: 61st Annual International Conference and Exhibition, EAGE, Extended Abstracts, cp-132-00182, doi: 10.3997/2214-4609.201407779.
Naville, C., S. Serbutoviez, A. Throo, O. Vinck, and F. Cecconi, 2004, Seismic while drilling (SWD) techniques with downhole measurements, introduced by IFP and its partners in 1990–2000: Oil & Gas Science and Technology, **59**, 371–403, doi: 10.2516/ogst:2004027.
Poletto, F., 2005, Energy balance of a drillbit seismic source — Part 2: Drillbit versus conventional seismic sources: Geophysics, **70**, no. 2, T29–T44, doi: 10.1190/1.1897039.
Poletto, F., A. Goertz, C. Bellezza, E. V. Bergfjord, P. Corubolo, J. E. Lindgård, and L. M. Moskvil, 2022, Seismic-while-drilling by drill-bit source and large-aperture ocean-bottom array: Geophysics, **87**, no. 2, D33–D45, doi: 10.1190/geo2021-0020.1.
Poletto, F., M. Malusa, and F. Miranda, 2001, Numerical modeling and interpretation of drillstring waves: Geophysics, **66**, 1569–1581, doi: 10.1190/1.1487102.
Poletto, F., and F. Miranda, 2004, Seismic while drilling: Fundamentals of drillbit seismic for exploration: Elsevier.
Poletto, F., F. Miranda, P. Corubolo, A. Schleifer, and P. Comelli, 2014, Drill bit seismic monitoring while drilling by downhole wired-pipe telemetry: Geophysical Prospecting, **62**, 702–718, doi: 10.1111/1365-2478.12135.
Poletto, F., F. Miranda, B. Farina, and A. Schleifer, 2020, Seismic-while-drilling drillbit source by ground force: Concept and application: Geophysics, **85**, no. 3, MR167–MR178, doi: 10.1190/geo2019-0449.1.
Poletto, F., F. Rocca, and L. Bertelli, 2000, Drill-bit signal separation for RVSP using statistical independence: Geophysics, **65**, 1654–1659, doi: 10.1190/1.1444853.
Rector, J.W., III, and B. P. Marion, 1991, The use of drillbit energy as a downhole seismic source: Geophysics, **56**, 628–634, doi: 10.1190/1.1443079.
Saputelli, L., M. Economides, M. Nikolaou, and V. Kelessidis, 2003, Real-time decision-making for value creation while drilling: Middle East Drilling Technology Conference and Exhibition, SPE/IADC.
Silvestrov, I., A. Bakulin, E. Hemyari, A. Aldawood, and A. Egorov, 2021a, Seismic-while-drilling with a pilot signal from a downhole memory-based vibration sensor: First International Meeting for Applied Geoscience & Energy, Expanded Abstracts, 3058–3062, doi: 10.1190/segam2021-3582705.1.
Silvestrov, I., E. Hemyari, A. Bakulin, Y. Luo, A. Aldawood, F. Poletto, Y. Liu, Y. Du, A. Egorov, and P. Golikov, 2021b, Processing of seismic-while-drilling data from DrillCAM system acquired with wireless geophones, top-drive and downhole vibrations sensors: Middle East Oil & Gas Show and Conference, SPE, Extended Abstracts, SPE-204543-MS.
Staron, P., G. Arens, and P. Gros, 1988, Method of instantaneous acoustic logging within a wellbore: U.S. Patent 4,718,048.
Vieitez, C., and M. Cox, 2017, Walkaway seismic-while-drilling operation delineates salt dome: Offshore 77, https://www.offshore-mag.com/production/article/16755923/walkawayseismicwhiledrilling-operation-delineates-salt-dome, accessed 17 April 2022.

Biographies and photographs of the authors are not available.

DOI:10.1190/geo2022-0031.1